Influence of geosynthetic-interlayers on the performance of asphalt overlays on pre-cracked pavements

Sireesh Saride[1*] and Vinay Kumar V[2]

[1]Associate Professor, Department of Civil Engineering, Indian Institute of Technology Hyderabad, Telangana-502285, India, sireesh@iith.ac.in.

[2]Doctoral student, Department of Civil Engineering, Indian Institute of Technology Hyderabad, Telangana-502285, India, christite.vinay@gmail.com.

[*]Author for Correspondence.

Address for Communication:

Associate Professor

207, Academic Block A,

Department of Civil Engineering

Indian Institute of Technology Hyderabad

Kandi, Sangareddy

Telangana – 502 285, India

Tel: +91 40 2301 6066

For possible publication in

Geotextiles and Geomembranes

Influence of geosynthetic-interlayers on the performance of asphalt overlays on pre-cracked pavements

Abstract

The functions of geosynthetic-interlayers in retarding reflection cracking and improving fatigue performance of hot mix asphalt (HMA) overlays in flexible pavements are evaluated in this study. The delamination or debonding mechanisms of the overlays are studied when geosynthetic-interlayers are adopted. A polyester grid coated with polymer modified binder (G1), a woven geo-jute mat (G2), and a bi-axial polypropylene grid (G3) interlayer are examined based on their adhesion properties. A two stage experimental program is reported. During the first stage, the performance of the geosynthetic-interlayers sandwiched between the pre-cracked old pavement and new asphalt layers are evaluated using flexural fatigue testing. A digital image correlation (DIC) technic was employed to record the failure modes and the corresponding tensile strains in the overlay system. During the second stage, the effect of interlayers on the interface bond strength was evaluated with the help of shear and tensile bond strength tests. The results show that the inclusion of interlayers retard the propagation of reflection cracking, however, results in the delamination of overlays. The debonding effect is prominent in G3 interlayers due to their high initial stiffness. Overall, interlayers with high interfacial shear and pull-off tensile bond properties proved effective in controlling the reflection cracking and increasing fatigue life of the overlays.

Keywords: *Geosynthetics, HMA overlays, reflection cracking, flexural fatigue testing, interface bond strength.*

1. INTRODUCTION

The hot mix asphalt (HMA) overlays, generally referred to as asphalt overlays, is the common and convenient rehabilitation technic available to restore the serviceability of the existing pavement surface. It is often observed that these overlays are associated with reflection cracking problems. Reflection cracking may be defined as a process of propagation of discontinuities or cracks from the existing distressed layer through the new overlay under traffic and temperature induced stresses (Cleveland et al. 2002; Kim and Butlar, 2002). The thickness of the overlay is also one of the factors responsible for reflection cracking (Goulias and Ishai, 1999). Reflection cracking causes premature failure of overlays, and then the entire pavement system by allowing moisture into the subsequent layers underneath via cracks (Elseifi and Al-Qadi, 2003; Farshad, 2005; Smith, 1983). The reflection cracking is a very complex phenomenon, which cannot be completely arrested, however, various technics are available to resist the crack propagation. The most common technic is to provide an interlayer at the interface of an old and new pavement layers. In general, fabrics or geotextiles, geogrids, composites and stress absorbing membrane interlayers (SAMI) are adopted for this purpose. The interlayers improve the performance of the overlays by providing stress relief, reinforcement and moisture control (Elseifi, 2003). However, the interlayer should possess sufficient cross-sectional area and modulus to improve the strength and performance of the overlays (Lytton, 1989). Hence, a proper understanding of the behavior of interlayers in retarding the reflection cracks is necessary to select an appropriate interlayer for a given pavement system.

2. BACKGROUND

A large number of laboratory, field and numerical studies were performed to evaluate the effectiveness of various interlayer systems to retard the reflection cracks. The location of an interlayer in a pavement system is crucial in absorbing tensile strains mobilized during loading. When placed at the interface of an old and new overlay, interlayers effectively absorb the tensile strains and reduces the vertical deformation and there by the crack propagation (Brown et al. 2001; Khodaii et al. 2009; Li et al. 2016; Moayedi et al. 2009). The fatigue life, bending strength and crack-resisting potential was observed to improve when the fiberglass grid interlayer was placed at the bottom of asphalt layer (Guo and Zhang, 1993; Fallah and Khodaii, 2015; Virgili et al. 2009). A paving fabric or geotextile interlayer system, which provides stress relief and moisture control functions, was found effective in improving the pavement performance (Farshad, 2005). The fabric interlayers were also found cost-effective when compared to the thick asphalt overlays (Steen, 2004). The inclusion of geosynthetic-interlayers not only improves the performance of HMA overlay in terms of reducing the rate of reflective cracking in overlays but also increase the resistance to rutting (Correia and Zornberg, 2016; Goulias and Ishai, 1999; Khodaii et al. 2009). The effects of geosynthetic-interlayers on reflective crack retardation were evaluated under laboratory conditions by Caltabiano (1990), El Meski and Chehab (2013), Gonzalez-Torre et al. (2015), Sanders et al. (1999) and Walubita et al. (2015). They found that the interlayers improved the performance life of the overlays effectively by resisting the crack propagation. Ogundipe et al. (2012) found SAMIs to be effective in retarding the crack propagation only at low load levels. Similarly, Kim et al. (2010) and Pasquini et al. (2014, 2015) found that the appropriate

selection and application of optimized grid-reinforced bituminous membrane (composites) can significantly enhance the reflective cracking resistance in asphalt pavements. Barraza et al. (2010) and Nejad et al. (2016) evaluated the durability of various anti-reflective cracking systems including geotextiles, geogrids and SAMI layers under cyclic loads and found that all the interlayer types reduced the reflective cracking process and geogrids were found to be most effective. A similar type of result for grids was obtained by Brown et al. (2001) and Canestrari et al. (2013); however, Brown et al. (2001) and Pasquini et al. (2014, 2015) observed that there was a reduction in shear resistance for specimens with geosynthetic-interlayers. The reduction in the shear resistance was observed to be minimal in the case of geogrids and the reason was attributed to the presence of apertures. On the other hand, Barraza et al. 2010; Brown et al. 2001; and Caltabiano and Brunton, 1991 have shown that the interlayers without the apertures (geotextiles) have proven least shearing resistant. The interlayer bonding is found to be improved when interlayers are coated with an appropriate binder or activated epoxies (Aldea and Darling, 2004; Ferrotti et al. 2012).

From the literature, it can be often noted that the geosynthetic-interlayers are placed in a two layer (new asphalt layers), i.e. the interlayers were provided between the two new asphalt layers, but not at the interface of an old and new asphalt layers. However, the general practice is to place the interlayer with an appropriate tack coat at the interface. In addition, a mixed performance of the interlayers was witnessed, when placed in a new asphalt overlay. Hence, the current study aims to replicate the field scenario in the laboratory while testing an aged and cracked old pavement layer, which was extracted from a distressed pavement, reinforced with geosynthetic-interlayers and asphalt overlays. The objective is to evaluate the

performance of the interlayers against the crack propagation into the overlays under cyclic four point bending tests with the aid of digital image correlation technic. The interface bonding of interlayers with the old and new pavement layers is also evaluated to understand the various parameters affecting the interface bond strength.

3. MATERIALS AND SAMPLE PREPARATION

To prepare two-layer asphalt beams with and without interlayers shown in Fig. 1, asphalt, tack coat (binder) and different types of geosynthetic-interlayers, shown in Fig. 2, were used. Following sections discuss the index and engineering properties of these materials.

3.1. Asphalt

The asphalt, also known as asphalt concrete and bituminous concrete, consists of a bitumen binder and aggregates and a filler material which are mixed thoroughly in a mixing plant. Two-layer asphalt concrete beams consists of a new asphalt concrete overlay compacted over an old pavement layer as shown in Fig. 1. The old pavement's surface layer was cut and carefully extracted from an existing state highway during the rehabilitation process. The old asphalt concrete cake was cut into required sizes for the testing. The upper layer consisted of asphalt concrete with a nominal aggregate size of 13 mm. The asphalt concrete mix was prepared in the mixing plant and transported to the laboratory. The mix comprises of a penetration grade (PG) 60/70 bitumen with an optimum binder content of 5.5% by weight of the aggregate as determined by Marshall-stability test. The HMA concrete has a maximum strength of 14.25 kN and a flow value of 2.5 mm as per the Marshall-stability test.

3.2. Binder tack coat

Tack coat materials generally employed are either bitumen emulsions or cutbacks, whereas, the bituminous emulsions are the most commonly used tack coat material in both rehabilitation and new projects. The application of asphalt cement as a tack coat at the interface with geosynthetic-interlayers was proved to improve the interface bond strength (Button and Lytton 1987). Hence, the asphalt binder of the same grade as that used in the HMA overlay was used as a tack coat in this study. The physical properties of the tack coat are presented in Table 1. The viscosity of the binder was determined in a Brookfield viscometer at 60 ^{o}C. Based on the penetration value of 66, the binder tack coat is classified as a bituminous binder of PG 60/70.

3.3. Geosynthetic-interlayers

Three types of geosynthetic-interlayers viz. a polyester grid, a woven jute mat and a biaxial polypropylene grid were considered in the current study (Fig. 2). These materials were selected based on the material type, aperture size and other tensile characteristics to investigate their influence in interface shear, tensile bond strength and fatigue characteristics. A wide width tensile strength test was performed according to ASTM D4595 (2011) on the geosynthetic-interlayers on both machine direction (MD) – which would be along the length of the road, and cross- machine direction (CMD) - across the width of the road. These tests were conducted initially at room temperature (25 ^{o}C) and repeated after a temperature test. In the temperature tests, the geosynthetic-interlayers were heated up to 150 ^{o}C for 2 hrs. and then reduced to room temperature for 24 hrs. The latter exercise is to verify the influence of temperature on the working properties of the geosynthetics which are typical during the

construction process, where the typical temperature of the asphalt concrete would be in the range of 135 ^{o}C – 150 ^{o}C. Figures 3a and 3b show the variation of the tensile strength of the geosynthetic materials obtained at 25 ^{o}C and after the temperature test respectively along machine and cross machine directions. The properties of geosynthetic-interlayers used in the study are as follows:

Polyester grid (G1): The grid is manufactured using a high molecular weight and high tenacity polyester yarns. The high tenacity yarns are knitted to form a geogrid material having an aperture size of 18 mm as shown in Fig. 2a. The polyester grid is coated with a polymeric modified bitumen layer. It is expected that the polymeric modified bitumen layer offers a high bondage between the old and new asphalt layers. The polyester grid is a 2 mm thick material (including the bitumen coating) with a square aperture opening of 18 mm. The tensile strength of the polyester grid (G1) is about 48 kN/m and 52 kN/m along MD and CMD respectively, however, there is no considerable reduction in tensile strength after the heating test. The failure strain of this material is observed to be about 18-20% at room temperature, and it has increased to 32-34 % after the temperature test (see Fig. 3).

Woven geojute mat (G2): The mat is manufactured out of natural jute materials like fibers and/or threads. The fibers are woven naturally or by the machine to form a mat without any apertures as shown in Fig. 2b. The tensile strength of the material is 25 kN/m (MD) at 5% strain and 20 kN/m (CMD) at 13% strain (Fig. 3). The influence of temperature is found to be negligible on the geojute mat.

Biaxial polypropylene grid (G3): The biaxial grid is made up of 4 mm thick polypropylene material with a 40 mm square aperture (Fig. 2c). The tensile strength of the biaxial grid is

about 42 kN/m (CMD) and 36 kN/m (MD) at 10-12% failure strain. The G3 interlayers have shown a drastic reduction in ultimate tensile strength of about 29% in machine direction and 37% in cross machine direction, without any change in the initial stiffness.

3.4. Two-layer asphalt concrete specimen preparation:

The two-layer asphalt concrete specimens for repeated load four-point bending tests were prepared using a static weight compactor weighing 5 kg having a constant height of fall of 50 cm. The sample preparation consisted of placing an old pavement layer of size 400 mm (length) × 300 mm (width) × 45 mm (thickness) as a bottom layer in a steel mold. Then a bitumen of PG 60/70 was applied at a residual rate of 0.25 kg/m^2 on the old pavement layer as a tack coat and allowed for emulsion breaking as per the ministry of road transport and highways (MORTH) specifications (MORTH, 2003). Then, in the case of controlled specimens, which are referred as NG specimens, a 45 mm thick HMA layer was compacted over the old pavement block. The air void content in the HMA layer was theoretically calculated as 7%, which is slightly above the general range of 3-6% for asphalt concrete layers. The difference may be attributed to the compaction methodology adopted in this study against the gyratory compaction. In the case of geosynthetic-interlayered specimens, the interlayer was placed after the emulsion breaking time, which was obtained as 30 min in prior trials. Figure 1b shows the schematic of a two-layer asphalt beam specimens with an old pavement layer, tack coat, interlayer and HMA overlay prepared in the laboratory. The old pavement layer and the new overlay can be clearly distinguished by their color (Fig.1a). The two-layer asphalt beams of size 400 mm (length) × 50 mm (width) × 90 mm (thickness) were then cut from the slabs prepared. To replicate a crack in an old distressed pavement surface

layer, a notch was introduced in the bottom layer of the asphalt concrete beams. Two different notch depths viz. 25 mm and 40 mm, approximately accounting for 55 % and 90 % of the thickness of the old pavement, were considered to investigate the influence of the crack depth on the overall performance of the geosynthetic-interlayers.

Further, for the digital image analysis, a speckle pattern was created on the face of the asphalt beams by coating the surface completely with a white paint followed by spraying a black paint. The speckle pattern helps to determine the displacement and strain fields in the specimens during the fatigue testing, which are otherwise difficult to obtain using the strain gauges.

Similarly, the asphalt concrete specimens of dimensions 300 mm (length) × 300 mm (width) × 90 mm (thickness) were prepared as per the procedure mentioned above for interface shear strength tests with and without interlayers.

4. TESTING PROGRAM

The testing program has been divided into two stages as shown in Table 2. During the first stage, pre-cracked (with 25 mm or 40 mm crack depth), two-layer asphalt beams with and without geosynthetic-interlayers were investigated to estimate the crack-resisting potential under flexural fatigue four point bending tests. In this test, the resistance against the crack propagation into the new asphalt overlay was evaluated in terms of the total number of repeated load cycles completed effectively before reaching the failure. The failure is defined as a complete breakage of specimen at which, no further load is resisted by the specimen.

During the second stage, interface bond strength of the geosynthetic-interlayers were quantified under shear and tensile mechanisms. The interface shear strength was determined using an interface shear strength test, while, the interface tensile bond strength of the geosynthetic-interlayers and the tack coat combination was determined using adhesion tensile strength test.

4.1. Flexural fatigue test:

The flexural fatigue test was performed to investigate the effectiveness of two-layer asphalt specimen with and without geosynthetic-interlayers under repeated loading conditions as per ASTM D7460 (2010). The two-layer asphalt specimens with 25 mm and 40 mm deep and 10 mm wide notch were tested under a four point loading condition in a load controlled mode as shown in Fig. 4. The tests were performed at normal room temperature (25 ^{o}C) and repeated on duplicate specimens to verify the repeatability of the data. A continuous haversine type constant load pattern with a frequency of 1 Hz was applied to replicate the repeated traffic loading conditions i.e. equivalent single axle wheel contact pressure of 550 kPa. To simulate the contact pressure of 550 kPa, maximum load (P) to be applied on the specimen was back calculated from the maximum flexural stress equation (1) derived for the case as per ASTM D7460 (2010):

$$\sigma_f = \frac{PL}{bh^2} \quad (1)$$

Where, σ_f is the maximum flexural stress in MPa (= 0.550 MPa), P is the maximum load applied in kN, L is the length of the beam in m, b and h are the width and thickness of the beam in m. The maximum load (P) is calculated to be 0.6 kN. During the testing, a seating

load of 0.06 kN, which is 10 % of maximum load, and the maximum load of 0.6 kN were continuously applied and the corresponding vertical deformations at mid-span of the specimen were recorded. These vertical deformations were used to calculate the flexural strains at the bottom most layer of the asphalt beams.

The corresponding flexural strains can also be calculated using equation 2:

$$\epsilon = \frac{108\delta(h-t)}{23L^2} \quad (2)$$

Where, ϵ is the maximum flexural (tensile) strain in the sample, δ is the vertical deformation at mid-span of the sample in mm.

The applied constant load (P) and the calculated strain can be used to represent the flexural fatigue load-strain relationship of the two-layer asphalt beams. Note that the maximum flexural stress considerably varies during the test due to propagation of the crack; hence, the data is presented in terms of flexural fatigue load with strain. Figure 5 shows a typical flexural fatigue load-strain curve for two-layer NG asphalt beam with 25 mm crack depth. Notice that the flexural cyclic strain decreases with increasing number of load repetitions. This may be due to the reduction in the rate of permanent deformations in each cycle with number of load repetitions. The load-strain patterns obtained are different for specimens with different crack depths and interlayer type. The flexural test results for different cases are analyzed further and presented in the subsequent sections. Generally, the flexural fatigue test gives an idea of either fatigue life of the specimen under repetitive loading or the maximum flexural stress that can be applied on a beam. This test does not provide any information on the propagation of the existing cracks or crack development and

delamination of the interlayers during the testing process. Generally, the beams are instrumented with asphalt strain gauges to obtain localized information at critical positions. This method may not provide information at all the critical locations, especially when two layer laminated asphalt beams are employed. Hence, a continuous monitoring of complete strain fields across the specimen surface would provide a valuable information on the crack propagation, strains corresponding to the interface failure and critical tensile strains at the crack tip (Kumar and Saride, 2017; Safavizadeh et al. 2015).

In this study, the strain field in the specimens at different load cycles was investigated using a two-dimensional, full field optical technic known as digital image correlation (DIC). The DIC technic is an optical data analysis method, which employs a mathematical correlation technic to measure the changes in a series of images accurately. The correlation between the un-deformed pattern of the reference image and the deformed pattern of the images are used to obtain the two-dimensional full field displacements. The displacement fields are then computed through gray level correlations between the reference image and the images with deformed patterns using a commercial software (VIC-2D). The strain fields are then computed from the gradients of displacement fields obtained. Figure 4 shows the area on the specimen considered for the DIC analysis. The selected region was continuously focused and the images were recorded at various load cycles until the failure.

4.2. Interface shear strength test:

A large scale interface shear test device used in the current study (Fig. 6) is in compliant with ASTM D5321 (2008). The two-layer asphalt samples were prepared in the two half boxes separated by an interface zone as explained in section 3.4. A constant horizontal

displacement rate of 1 mm/min was applied along with a constant normal load perpendicular to the interface zone. The tests were repeated twice for different normal stress conditions viz., 30 kPa, 60 kPa and 120 kPa at a test temperature of 25 ^{o}C. The data obtained from the test in terms of shear stress and horizontal displacements were analyzed for interface shear characteristics.

4.3. Adhesion tensile test (ATT):

The interface tensile bond strength between the tack coat and the interlayer is very critical as the tack coat is found to be the weakest zone during a pavement failure due to improper bonding. An adhesion tensile test (ATT) apparatus compliant with ASTM D4541 (2002) is modified and fabricated in-house for the current study to determine the pull-off tensile strength of the tack coat applied on the geosynthetic-interlayers. The test setup consists of two 100 mm size square plates, one with an opening at the center, to accommodate the pull-stub attached on to the geosynthetic material.

The geosynthetic-interlayers cut into 100 mm square grid size were placed in between the two steel plates and clamped by mechanical bolting. A binder tack coat of about 0.08 g was heated up to a temperature of 135 ^{o}C and applied on the geosynthetic material exactly at the center and a pull stub of known diameter was hardly pressed against it (Ferrotti et al. 2012).

The whole assembly of pull stub and the plates were then conditioned at a test temperature for 24 hours before placing the pull-stub assembly in the universal testing machine as shown in Fig. 7. The ATT test was performed at three different temperatures viz. 20 ^{o}C, 30 ^{o}C and 40 ^{o}C as the interface tensile bond strength is highly sensitive to the temperature. A tensile

load was applied at a constant displacement rate of 1 mm/min until the pull-stub gets completely detached from the interlayer material and the corresponding peak load was noted. The pull-stub diameter and the tensile pull-off load with respect to the displacement data is analyzed to obtain the interfacial tensile bond strength.

5. RESULTS AND DISCUSSIONS

5.1. Flexural fatigue test results

The flexural fatigue test conducted in a load controlled mode helps to investigate the influence of the geosynthetic-interlayer on resisting the crack propagation in a pre-cracked asphalt beam specimen. The applied cyclic flexural stress causes a continuous increase in the flexural strain until the specimen does not sustain any further load cycles (N) causing a complete fracture in the specimen. The results obtained from the flexural fatigue tests on two-layer asphalt beams with 25 mm and 40 mm crack depths are presented in Fig. 8, which depicts the variation of vertical deformations with number of load cycles (N). In both the configurations, the unreinforced (NG) specimens failed to resist a large number of load repetitions before the crack propagated into the overlay. However, as expected, the specimens with 25 mm deep notch have sustained higher number of load repetitions than the specimens with 40 mm notch depth. Contrarily, the specimens with geosynthetic-interlayers have resisted vertical deformations for a large number of load repetitions. This indicates that the specimens with interlayers have improved the performance of the asphalt overlays by restricting the vertical deformations and crack propagation. In addition, the geosynthetic-interlayer with relatively low initial stiffness (G1) has performed superior than the interlayer with high initial stiffness (G3) as shown in the Figs. 3a and 3b. This could be due to the

smooth transfer of strain energy from the cracked pavement to the geosynthetic-interlayer, which has near similar elongation properties, resulted in initiating the membrane effect in G1 interlayer. To mobilize this effect in the case of stiffer interlayers such as biaxial geogrid specimens (G3), excessive deformations are necessary. It can be inferred from Fig. 8 that the vertical deformations required for the G3 specimen are higher than the G1 specimen at all load repetitions. For instance, at 100 load cycles, the vertical deformation in G1 and G3 specimens were respectively, 2.5 and 5.8 mm, i.e. about 66 % higher deformations are required to mobilize the membrane effect in the case of stiffer geosynthetic-interlayers. The other possible reason for the inferior performance of G3 interlayers could be attributed to their high initial stiffness, which reduces the interfacial bonding between the pavement layers (Graziani et al. 2014). However, the thermal effect on the interlayers plays an important role in their performance as well (Gonzalez-Torre et al. 2014; Norambuena-Contreras et al. 2016).

To investigate the effectiveness of interlayers in improving the fatigue life of two-layer asphalt specimens, a non-dimensional performance indicator known as improvement ratio (I_R) is introduced. The improvement ratios are calculated at different vertical deformations of the asphalt beams. The I_R is expressed mathematically as shown in equation 3.

$$I_R = \frac{N_I}{N_U} \tag{3}$$

Where, N_I is the number of load cycles sustained by samples with interlayer before failure at a given vertical deformation and N_U is the number of load cycles sustained by samples without interlayer before failure at the same vertical deformation.

Figure 9 shows the improvement ratio for specimens with various interlayers for both test configurations (25 mm crack depth and 40 mm crack depth) at different vertical deformations. Though the expected vertical deformations are low on a pavement during the traffic loading, higher vertical deformations are considered in this study as an academic exercise. The improvement ratio has increased with an increase in the vertical deformation for all the test configurations. However, the performance improvement is observed to be higher in the specimens with deeper initial crack (40 mm) than the shallow initial crack (25 mm). Besides, the stiffness modulus of the beams with shallow cracks is generally higher than the beams with deeper cracks. Hence, the former beams have sustained a higher number of load repetitions than the latter ones without interlayers, thus the decrease in the improvement ratio. It can be clearly seen that for the G1 interlayer specimen with 40 mm crack, an improvement ratio of about 14 is observed against about 6 for 25 mm crack at 6 mm vertical deformation. It can also be inferred that for G1 specimen with 40 mm crack depth, the improvement ratio drastically increased after 4 mm vertical deformation. At 4 mm deformation, the crack would have reached the interlayer and the specimen has resisted a higher number of load repetitions due to the transfer of the strain energy to the interlayer as discussed earlier.

Based on the image analyses, the deformation fields are calculated for a different number of load cycles and the variation of deformation field along the vertical direction are plotted as deformation bands as shown in Fig. 10. In each color band, the vertical deformations are uniform. The image analysis considers the downward deformation as negative. It can be visualized that the deformation band at the mid-span of the beams show a maximum value

due to the maximum curvature of the beam at failure. Note that the deformation bands in the NG specimen are continuous throughout the depth of the beam, indicating that the deformations are uniform throughout the depth (Fig. 10). Whereas, the deformation bands are discontinuous at the interface in all the specimens with geosynthetic-interlayers. The discontinuities in the deformation bands are due to the presence of interlayers at the interface zone, which restrains the crack propagation into the overlay and controls the vertical deformation. Hence, maximum vertical deformations are observed in the bottom layer, below the interlayer zone.

The presence of interlayer also helps to minimize the crack propagation in the vertical direction by controlling the maximum tensile strain at the crack tip. The tensile strain contours in all the specimens at failure are presented in Fig. 11 and it can be observed that the tensile strain for the NG specimen is very high (about 30 %). Whereas, the specimens with interlayer are observed to have a less tensile strain at the crack tip, due to the presence of interlayers. The interlayers absorb the tensile stresses mobilized from the cracks and restrict their propagation in the vertical direction. However, the cracks are observed to propagate in the horizontal direction at the interface zone at ultimate fatigue life of the beams (see Figs. 10 and 11). This horizontal crack propagation phenomena reduces the bondage between the old and new layers at the interface and leads to delamination of pavement layers at the interface zone.

Figure 12 shows the tensile strains obtained from the DIC analysis and the strains calculated from the equation 2 for the specimens with 25 mm crack depth. The tensile strains calculated are at the bottom layer of the beam, just above the crack tip as per the equation.

The tensile strains obtained from the image analysis are at the tip of the crack. It can be observed that the strains obtained from both the analyses seem to correlate very well with each other until the failure. However, at the time of failure, the tensile strains in the specimen are very high at the crack tip, which are very well captured from the image analysis. The tensile strain data at the failure are very high (about 30 %) in the NG specimen as shown in Fig. 12(a) than the specimens with geosynthetic-interlayers as shown in the Figs. 12(b), 12(c) and 12(d). The reduction in the tensile strains, as depicted from the Figs. 12 b – d, is due to the presence of the interlayers, which absorbed the strains by mobilizing the membrane effect. From Fig. 12, it is also very clear that the G1 specimen has performed well in controlling the tensile strains and improving the fatigue life of the asphalt overlays.

5.2. Interface shear strength test results

As can be witnessed from the flexural fatigue tests, the life of the HMA overlays is completely dependent on the relative behavior of the old and new layers at their interface. The fatigue life of the overlays seem to improve considerably with the inclusion of geosynthetic-interlayers; however, the bonding between the interlayer and the old and new asphalt layers is a crucial factor. Hence, to address these issues and to quantify the interfacial bond strength (τ_{max}) of various interlayers sandwiched between the old and new layers, interfacial shear tests were conducted.

The variation of interface shear stress with normal stress applied on the specimens is presented in Fig. 13. The peak interfacial shear strength envelopes (τ_{max}) can be calculated using the equation 4.

$$\tau_{\max} = C_0 + \sigma \tan \phi_p \quad (4)$$

Where, C_0 is the cohesion at pure shear condition, σ is the normal stress applied and ϕ_p is the peak friction angle.

The interface shear strength properties for various interface configurations tested at room temperature (25 ^oC) are presented in Table 3. The cohesion component seems to be high in the case of unreinforced two-layer asphalt specimens compared to the specimens with geosynthetic-interlayers. Among the geosynthetic-interlayered specimens, the cohesion component of G1 specimen is higher than the G3 specimen followed by G2 specimen. It is also observed that the interface shearing resistance is reduced when there is no direct contact between the old and the new layers, i.e. in the case of geo-jute mat interlayers. Similar observations were also noticed by Brown et al. (2001); Canestrari et al. (2006) and Ferrotti et al. (2012). From Fig. 13, it can be observed that the peak friction angle of G1, G2 and G3 interlayers are found to be about 40^o, 48^o and 42^o, respectively. The G2 interlayer has a higher friction angle owing to its surface properties compared to the other two interlayers as shown in Fig. 2. The interface shear strength (τ_{max}) of the interlayers is found to reduce with respect to the control specimen (NG). On an average, the reduction is observed to be about 17 %, 46 % and 32 % for G1, G2 and G3 specimens, respectively.

From the results, it is found that the NG interface condition has the highest interfacial bond strength and the inclusion of geosynthetic-interlayer at the interface reduces the bond strength. The reduction in bond strength may be attributed to the delamination of the old and new pavement layers due to weak bond at the interface. Hence, the bonding of the interlayers

with the existing old pavement and the new overlay plays a major role, which can be addressed from the interlayer's pull-off or adhesion tensile strength tests.

5.3. ATT results

The ATT results are obtained in the form of pull-off tensile strength expressed in MPa. The tests were conducted for different combinations of the geosynthetic materials with a single type of tack coat material. The tests were conducted at temperatures generally prevailed in the field conditions (20 ^{o}C, 30 ^{o}C and 40 ^{o}C), as the behavior of tack coat greatly depends on the temperature. The tests were repeated for 5 times in each case and the results are tabulated in Table 4.

From the current study, it is found that the bond strength increases with a decrease in the temperature as shown in Fig. 14. It can also be observed that the variation in the bond strength when the temperature increases from 30 ^{o}C to 40 ^{o}C is comparatively less than the variation in bond strength when the temperature increases from 20 ^{o}C to 30 ^{o}C. Among the interlayers tested, the G1 proved to be effective compared to the other types, due to the presence of a polymer modified binder coating on the grid, which helps to maintain a strong bond with the tack coat material. Although the surface of G3 interlayer is smooth, the bond strength appears to be superior to G2 interlayer. The amount of tack coat required in the case of G2 interlayer is comparatively higher than the other interlayer types, as it absorbs the binder tack coat due to the inherent absorbing nature of the jute material. These observations suggest that the tensile bond strength not only depends up on the temperature, but also on the material composition of the interlayers.

6. CONCLUSIONS

The performance of geosynthetic-interlayers in controlling reflection cracks and improving fatigue life of HMA overlays placed over pre-cracked old pavements was examined. A polyester grid coated with polymer modified binder (G1), a woven geo-jute mat (G2) and a biaxial polypropylene grid (G3) were adopted based on the aperture size, adhesion and tensile strength properties.

Initially, the fatigue life of geosynthetic-interlayered asphalt specimens was evaluated under a four point repeated loading condition. A DIC technic was employed to understand the crack propagation mechanism and to obtain the displacement fields and tensile strains at the crack tip. The flexural fatigue test results show that all the interlayers performed well in retarding the crack propagation in pre-cracked two-layer asphalt specimens. The binder coated polyester grid (G1) interlayer could resist the crack effectively compared to the other types. This is due to the stiffness, tensile strength and adhesion properties of the material. The influence of temperature on the tensile properties of G1 and G2 is negligible, whereas, the ultimate tensile strength of G3 interlayer has been reduced drastically by about 29% in machine direction and 37% in CMD. Besides, the high initial stiffness of G3 interlayer is responsible for delamination at the interface and there by the lower performance of this interlayer. The fatigue life of the asphalt specimens was higher for larger initial cracks (40mm crack depth) against shorter initial cracks (25 mm). As high as fifteen fold increase in fatigue life performance is noticed in the case of G1 interlayers against control specimens at 6mm vertical deformation.

The DIC results demonstrated that the cracks have propagated quickly to the surface in the controlled specimens, whereas, the specimens with geosynthetic-interlayers were effective in resisting the crack propagation. Based on the tensile strain fields on the specimens, the DIC technic could accurately identify the crack initiation and mobilization of membrane effect.

Later to analyze the interface shear strength properties and pull-off tensile bond strength of the interlayer, interface shear strength (ISS) tests and adhesion tensile strength tests (ATT) were performed. The ISS test results confirmed that the presence of an interlayer at the interface zone reduces the interface bond strength and eventually leads to debonding. The interface shear strength (τ_{max}) of the interlayers are found to reduce with respect to the control specimen (NG). On an average, this reduction is observed to be about 17%, 46% and 32% for G1, G2 and G3 specimens, respectively. The ATT study helps to understand the influence of the temperature and material composition on the interface pull-off bond strength values. The results show that the tensile bond strength for G1 interlayer type is high compared to all other types, irrespective of the temperature conditions. However, higher bond strength values are achieved when they are tested at a temperature of 25 ^{o}C. The ATT results also confirms the ISS test results that the performance of G1 interlayer superior to the other interlayers.

Overall, based on the flexural fatigue and interfacial bond strength test results, the interlayers performed very well in extending the fatigue life of the specimens before crack propagates and/or failure of the interface bond. The G1 interlayer with a polymer modified binder coating has shown a better performance in terms of higher fatigue life, interfacial bond strength and potential for retarding the reflection cracking.

References:

Aldea, C.M., Darling, J.R., 2004. Effect of coating on fiberglass geogrids performance. In: Proceedings of 5th International RILEM Conference on Reflective Cracking in Pavements: Mitigation, Risk Assessment and Prevention, Limoges, pp. 81-88.

ASTM D7460. 2010. Standard Test Method for Determining Fatigue Failure of Compacted Asphalt Concrete Subjected to Repeated Flexural Bending.

ASTM D4541. 2002 Standard Test Method for Pull-Off Strength of Coatings Using Portable Adhesion Testers. Annual Book of ASTM Standards, ASTM International, West Conshohocken, PA.

ASTM D4595. 2011. Standard Test Method for Determining Tensile Properties of Geotextiles by the Wide-Width Strip Method. Annual Book of ASTM Standards, ASTM International, West Conshohocken, PA.

ASTM D5321. 2008. Standard Test Method for Determining the Coefficient of Soil and Geosynthetic or Geosynthetic and Geosynthetic Friction by the Direct Shear Method. Annual Book of ASTM Standards, ASTM International, West Conshohocken, PA.

Barraza, D.Z., Peréz, M.A.C., Fresno, D.C., Zamanillo, A.V., 2010. Evaluation of anti-reflective cracking systems using geosynthetics in the interlayer zone. Geotext. Geomemb. 28(5), 483-489.

Brown, S.F., Thom, N.H., Sanders, P.J., 2001. A study of grid reinforced asphalt to combat reflection cracking. J. Ass. Asphalt Paving Technol. 70, 543-569.

Button, J.W., Lytton, R.L., 1987. Evaluation of Fabrics, Fibers, and Grids in Overlays. In: Proceedings of 6th International Conference on Structural Design of Asphalt Pavements. Vol. 1, Ann Arbor, Michigan, 925-934.

Caltabiano, M.A., 1990. Reflection Cracking in Asphalt Overlays. Thesis submitted to University of Nottingham for the Degree of Master of Philosophy.

Caltabiano, M.A., Brunton, J.M., 1991. Reflection cracking in asphalt pavement. J. Ass. Asphalt Paving Technol. 60, 310-330.

Canestrari, F., Grilli, A., Santagata, F.A., Virgili, A., 2006. Interlayer shear effect of geosynthetic reinforcements. In: 10th International conference on asphalt pavements, Québec.

Canestrari, F., Belogi, L., Ferrotti, G., Graziani, A., 2013. Shear and flexural characterization of grid-reinforced asphalt pavements and relation with field distress evolution. Mater. Struct. 48 (4), 959-975.

Cleveland, G.S., Button, J.W., Lytton, R.L., 2002. Geosynthetic in Flexible and Rigid Pavement Overlay. Texas Transport Institute, Texas A&M University System. Report. 1777-1.

Correia, N.S. Zornberg, J.G., 2016. Mechanical response of flexible pavements enhanced with geogrid-reinforced asphalt overlays. Geosynth. Intl. 23(3), 183-193.

Elseifi, M.A., 2003. Performance Quantification of Interlayer Systems in Flexible Pavements Using Finite Element Analysis, Instrument Response and Non Destructive Testing. PhD Thesis submitted to Virginia Polytechnic Institute and State University.

Elseifi, M.A., Al-Qadi, I.L., 2003. A Simplified Overlay Design Model against Reflective Cracking Utilizing Service Life Prediction. Transp. Res. Rec. J. Transp. Res. Board, 03-3285.

El Meski, F., Chehab, G.R., 2013. Flexural Behavior of Concrete Beams reinforced with Different Types of Geogrids. J. Mat. Civ. Eng. ASCE, 26(8).

Farshad, A., 2005. Potential Applications of Paving Fabrics to Reduce Reflective Cracking. Jackson State University, Mississippi. Federal Highway Report, FHWA/MS-DOT-RD-2005-174.

Fallah, S., Khodaii, A., 2015. Reinforcing overlay to reduce reflection cracking: an experimental investigation. Geotext. Geomemb. 43, 216-227.

Ferrotti, G., Canestrari, F., Pasquini, E., Virgili, A., 2012. Experimental evaluation of the influence of surface coating on fiberglass geogrid performance in asphalt pavements. Geotext. Geomemb. 34, 11-18.

Goulias, D.G., Ishai, I., 1999. Experimental System for Simulating Crack Propagation in Asphalt Pavements and Effectiveness of Geosynthetics in Crack Retardation. J. Testing Eval. JTEVA, 27(2), 106-113.

Gonzalez-Torre, I., Calzada-Perez, M. A., Vega-Zamanillo, A., Castro-Fresno, D., 2014. Damage evaluation during installation of geosynthetics used in asphalt pavements. Geosynth. Intl. 21(6), 377-386.

Gonzalez-Torre, I., Calzada-Perez, M. A., Vega-Zamanillo, A., Castro-Fresno, D., 2015. Experimental study of the behaviour of different geosynthetics as anti-reflective cracking systems using a combined-load fatigue test. Geotext. Geomemb. 43, 345-350.

Graziani, A., Pasquini, E., Ferrotti, G., Virgili, A., Canestrari, F., 2014. Structural response of grid-reinforced bituminous pavements, Mater. Struct. 47(8), 1391-1408.

Guo, Z., Zhang, Q., 1993. Prevention of cracking progress of asphalt overlayer with glass fabric. Reflective cracking in pavements: state of the art and design recommendations. Proceedings of 2nd International RILEM Conference, Liege, Belgium, 10–12, 398-405.

Kim, J., Buttlar, W.G., 2002. Analysis of reflective crack control system involving reinforcing grid over base-isolating interlayer mixture. J. Transp. Eng. 128 (4), 375-385.

Kim, H., Partl, M.N., Pimenta, R., Hean, S., 2010. Experimental Investigation of Grid-reinforced Asphalt Composites Using Four-Point Bending Beam Tests. J. Composite Mater. 44(5), 575-592.

Kumar, V.V., Saride, S., 2017. Evaluation of flexural fatigue behavior of two-layer asphalt beams with geosynthetic-interlayers using digital image correlation, Transp. Res. Rec. J. Transp. Res. Board. doi.10.3141/2631-06.

Li, P., Liu, J., Zhao, S., 2016. Performance of Multiaxial Paving Interlayer-Reinforced Asphalt Pavement. J. Mater. Civ. Eng. ASCE.

Lytton, R.L., 1989. Use of Geotextiles for Reinforcement and Strain Relief in Asphalt Concrete. Geotext. Geomemb. 8(3), 217-237.Moayedi, H., Kazemian, S., Prasad, A., Huat, B.B.K., 2009. Effect of Geogrid Reinforcement location in paved road improvement. Elect J. Geotech. Eng. 14.

MORTH, 2003. Specifications for Road and Bridge Works. Ministry of Road Transport and Highways, Indian Road Congress (IRC), New Delhi.

Nejad, F.M., Asadi, S., Fallah, S., Vadood, M., 2016. Statistical-experimental study of geosynthetics performance on reflection cracking phenomenon. Geotext. Geomemb. 44, 178-187.

Norambuena-Contreras, J., Gonzalez-Torre, I., Fernandez-Arnau, D., Lopez-Riveros, C., 2016. Mechanical damage evaluation of geosynthetics fibres used as anti-reflective cracking systems in asphalt pavements. Constr. Build. Mater. 109, 47-54.

Ogundipe, O.M., Thom, N., Collop, A., 2012. Investigation of crack resistance potential of stress absorbing membrane interlayers (SAMIs) under traffic loading. Constr.Build. Mater. 38, 658-666.

Pasquini, E., Bocci, M., Canestrari, F., 2014. Laboratory characterisation of optimised geocomposites for asphalt pavement reinforcement. Geosynth. Intl. 21(1), 24-36.

Pasquini, E., Pasetto, M., Canestrari, F., 2015. Geocomposites against Reflective Cracking in Asphalt Pavements: Laboratory Simulation and Field Application, Road Mater. Pavement Design, 16(4), 815-835.

Safavizadeh, S.A., Wargo, A., Guddati, M., Kim, Y.R., 2015. Investigating Reflective Cracking Mechanisms in Grid-Reinforced Asphalt Specimens. Transp. Res. Rec. J. Transp. Res. Board No. 2507, 29-38.

Sanders, P.J., Brown, S.F., Thom, N.H., 1999. Reinforced Asphalt for Crack and Rut Control. 7th Conference on Asphalt Pavements, Southern Africa.

Smith, 1983. Laboratory Testing of Fabric Interlayers for Asphalt Concrete Paving: Interim Report. Transp. Res. Rec. J. Transp. Res. Board No. 916, 6-17.

Steen, E.R., 2004. Stress Relieving Function of Paving Fabrics When Used in New Road Construction. Proceedings of 5th International RILEM Conference, Limoges, France, 105-112.

Virgili, A., Canestrari, F., Grilli, A., Santagata, F.A., 2009. Repeated load test on bituminous systems reinforced by geosynthetics. Geotext. Geomemb. 27, 187-195.

Walubita, L.F., Faruk, A.N.M., Zhang, J., Hu, X., 2015. Characterizing the cracking and fracture properties of geosynthetic-interlayer reinforced HMA samples using the Overlay Tester (OT). Constr. Build. Mater. 93, 695-702.

Table 1: Properties of binder tack coat

S. No.	Property	Values
1	Specific Gravity	1.01
2	Ductility (cm)	100+
3	Penetration ($1/10^{th}$ mm)	66
4	Viscosity, Brookfield at 60 ^{o}C (centipoise)	460
5	Softening point (^{o}C)	52
6	Flash point (^{o}C)	340
7	Fire point (^{o}C)	365

Table 2: Summary of experimental program

Stage	Test	Interface condition	Configurations
1	Four point bending test (Flexural fatigue)	NG, G1, G2 and G3	Specimens with 25 mm deep and 10 mm wide cracks
			Specimens with 40 mm deep and 10 mm wide cracks
2	Interface shear strength test	NG, G1, G2 and G3	Normal stresses: 30 kPa, 60 kPa and 120 kPa
	Adhesion tensile strength test	G1, G2 and G3	Test temperatures: 20 ^{o}C, 30 ^{o}C and 40 ^{o}C

Table 3: Peak envelope characteristics of interface shear strength test

S. No.	Interface type	Cohesion, C_0 (kPa)	Peak friction angle, ϕ_p (degrees)
1	NG	208.26	45.87
2	G1	173	40.28
3	G2	75.10	48.07
4	G3	128.18	42.09

Table 4: Interface bond strength results as per ATT

S. No.	Geosynthetic type	Temperature	Interface bond strength (MPa)					Mean bond strength (MPa)	SD	COV
			1	2	3	4	5			
1	G1	20 °C	3.34	3.96	3.67	2.98	3.45	3.48	0.37	0.13
		30 °C	2.48	1.96	2.16	2.86	2.54	2.40	0.35	0.12
		40 °C	2.37	1.65	1.49	2.01	1.97	1.90	0.34	0.12
2	G2	20 °C	1.87	2.34	2.02	1.68	2.15	2.01	0.25	0.06
		30 °C	1.48	1.06	1.88	1.35	1.78	1.51	0.33	0.11
		40 °C	1.25	1.38	1.62	0.86	1.01	1.22	0.30	0.09
3	G3	20 °C	2.46	2.87	2.35	1.96	3.01	2.53	0.42	0.18
		30 °C	1.7	2.43	1.64	1.36	1.58	1.74	0.41	0.16
		40 °C	1.35	0.96	1.24	1.58	1.46	1.32	0.24	0.06

Figure Captions:

Fig. 1: a) Photograph and b) schematic of two-layer asphalt concrete beams

Fig. 2: Geosynthetic-interlayers used in the study

Fig. 3: Tensile strength of geosynthetic-interlayers used in the study

Fig. 4: Four point bending (Flexural fatigue) test apparatus

Fig. 5: Typical fatigue load-strain curve for NG sample with 25 mm deep crack

Fig. 6: Interface shear strength test apparatus

Fig. 7: ATT setup placed in universal testing machine

Fig. 8: Variation of vertical deformation with number of load cycles

Fig. 9: Improvement ratio (I_R) for different interlayers

Fig. 10: Variation of vertical deformation bands for beams with 25 mm crack depth: DIC analysis at failure

Fig. 11: Typical DIC results for sample with 25 mm crack depth (a) Before testing, (b) Tensile strain contours at failure

Fig. 12: Tensile strains measured from DIC analysis and test data for sample with 25 mm crack depth (a) NG; (b) G1; (c) G2; and (d) G3

Fig. 13: Variation of interface shear stress with normal stress at a temperature of 25 ^{o}C

Fig. 14: Variation of interface tensile bond strength with temperature

(a) **(b)**

Fig. 1: a) Photograph and b) schematic of two-layer asphalt concrete beams

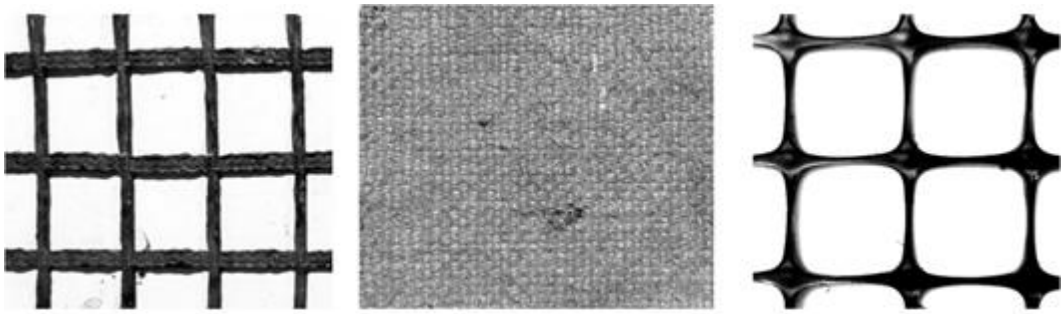

Fig. 2: Geosynthetic-interlayers used in the study

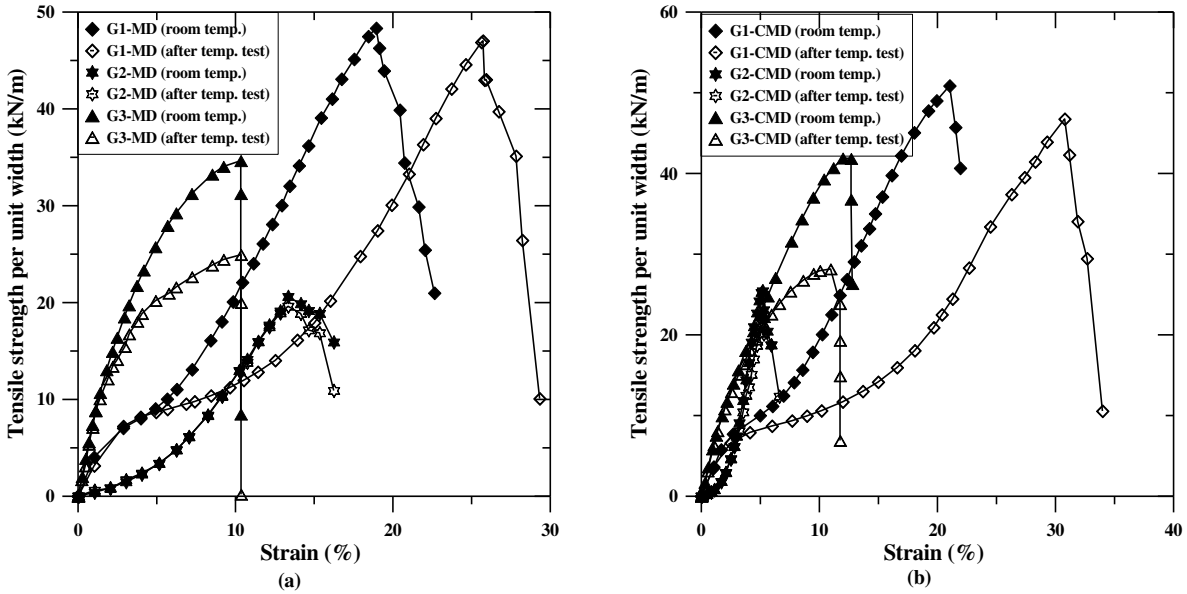

Fig. 3: Tensile strength of geosynthetic-interlayers used in the study

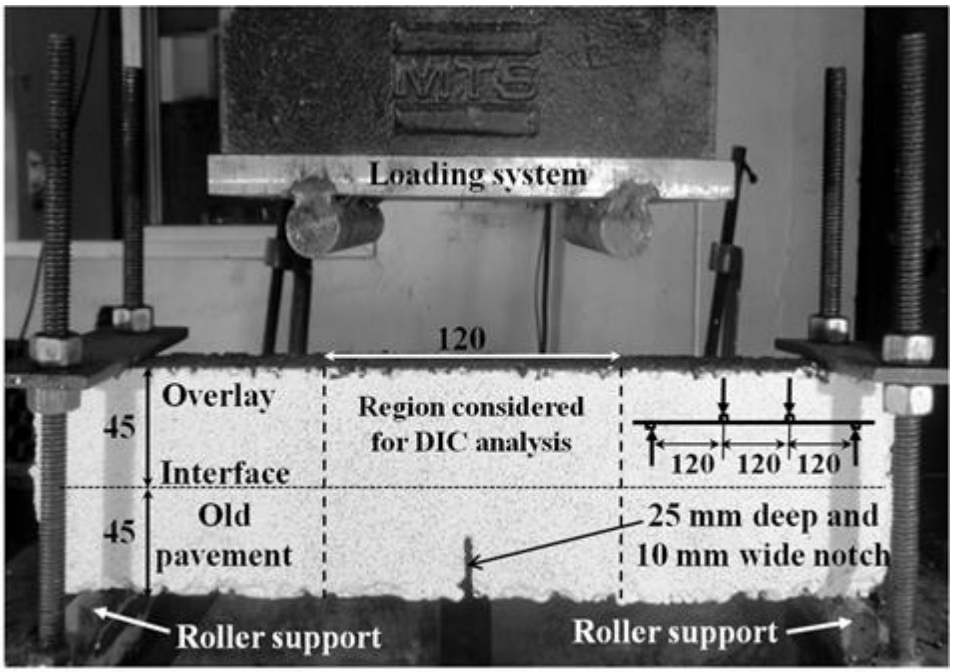

Fig. 4: Four point bending (flexural fatigue) test apparatus

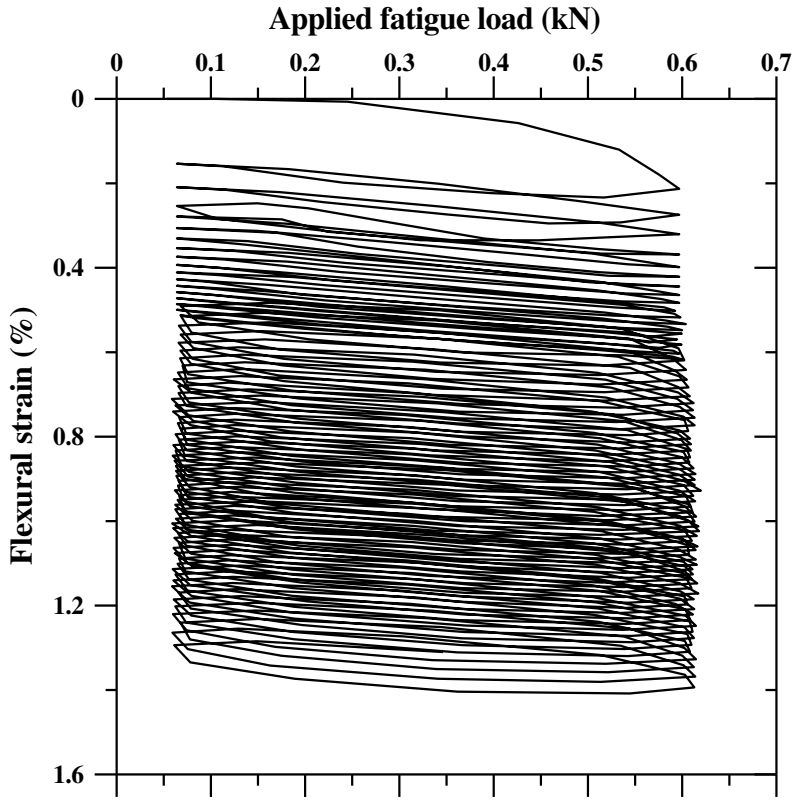

Fig. 5: Typical fatigue load-strain curve for NG specimen with 25 mm deep crack

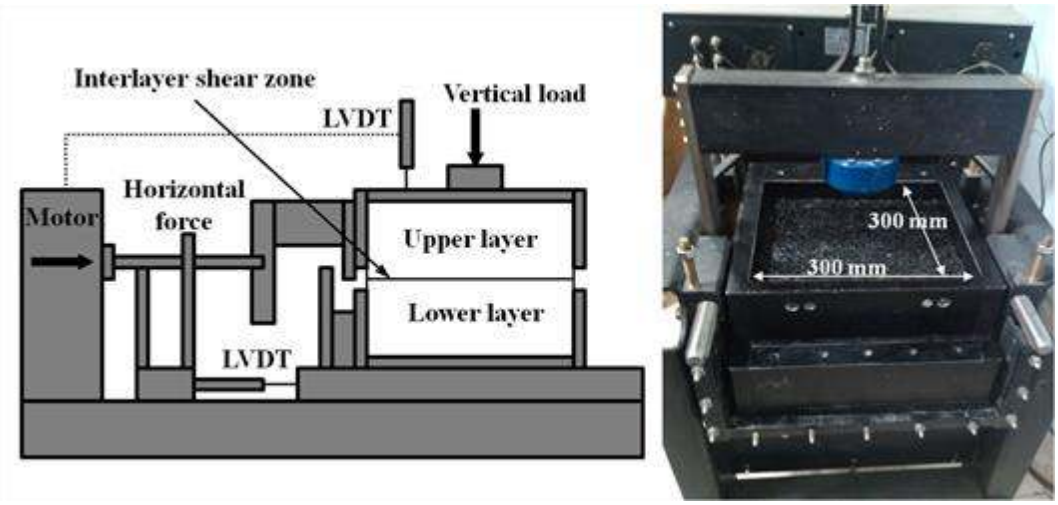

Fig. 6: Interface shear strength test apparatus

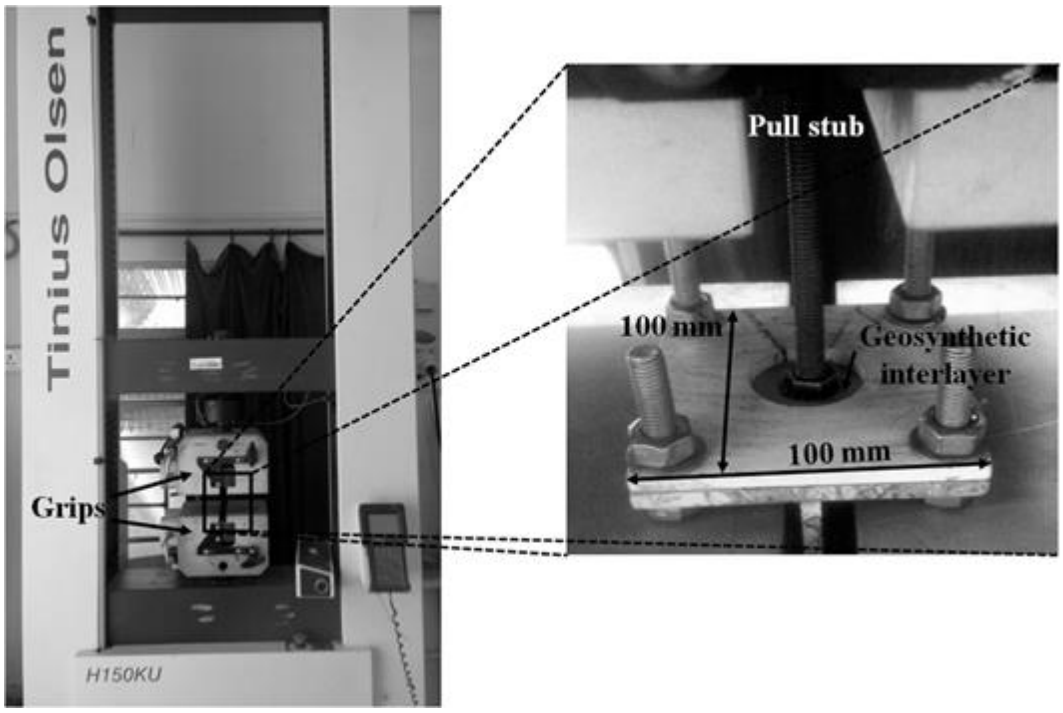

Fig. 7: ATT setup placed in universal testing machine

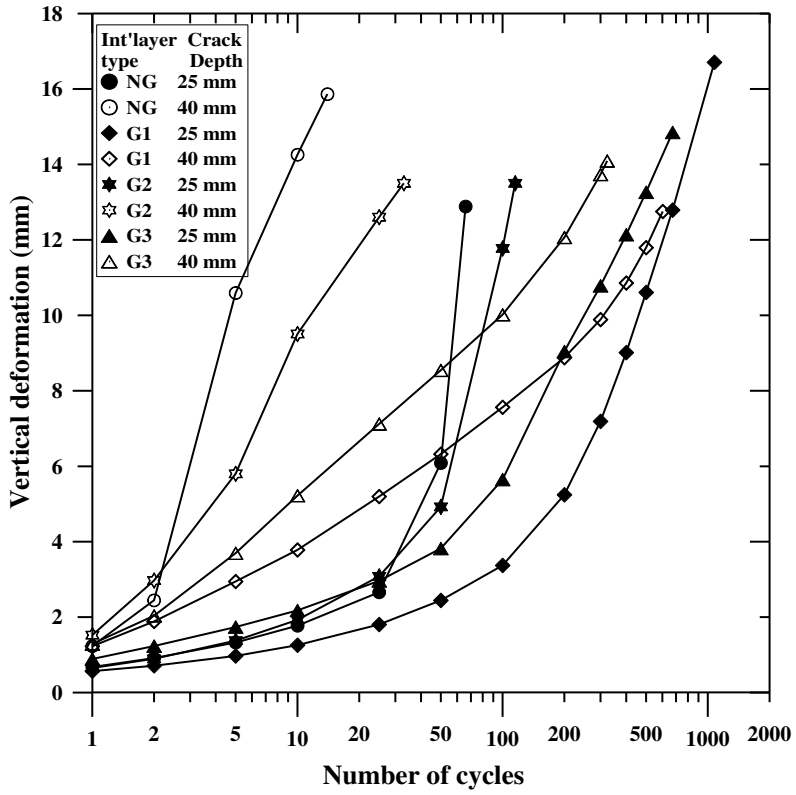

Fig. 8: Variation of vertical deformation with number of load cycles

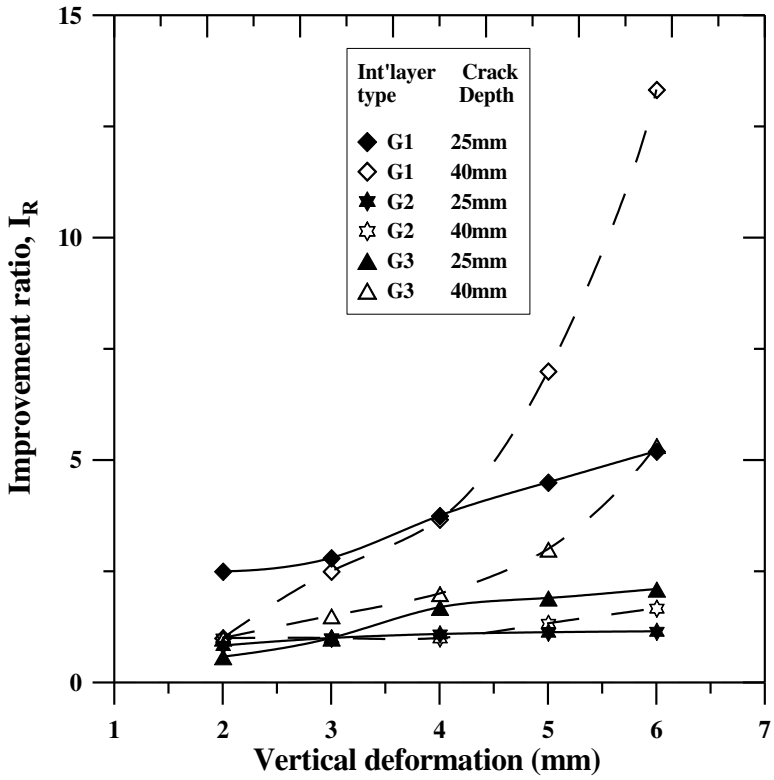

Fig. 9: Improvement ratio (I_R) for different interlayers

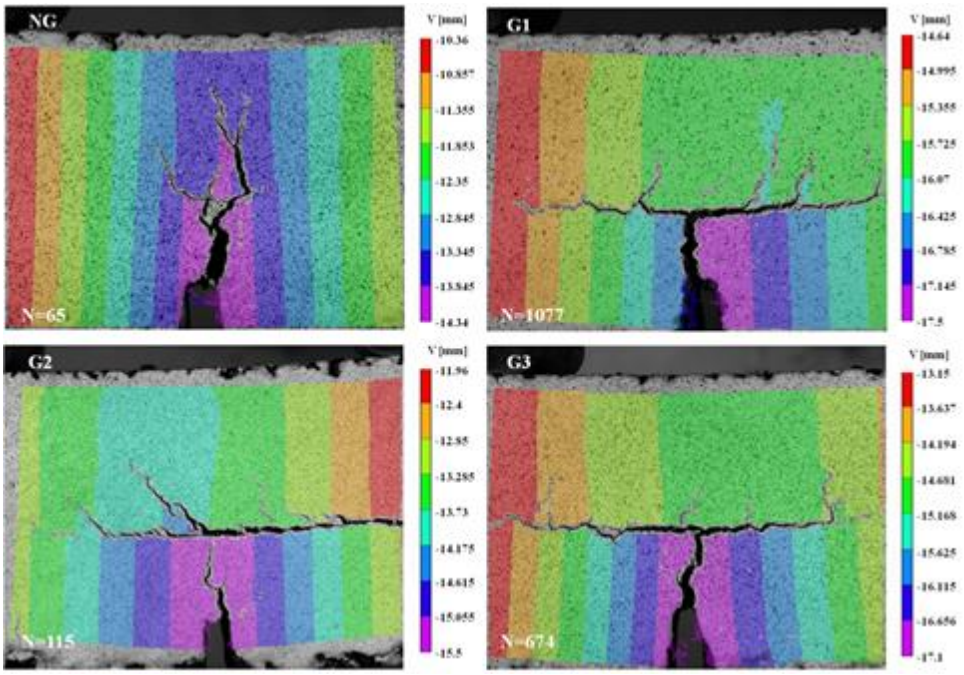

Fig. 10: Variation of vertical deformation bands for beams with 25 mm crack depth: DIC analysis at failure

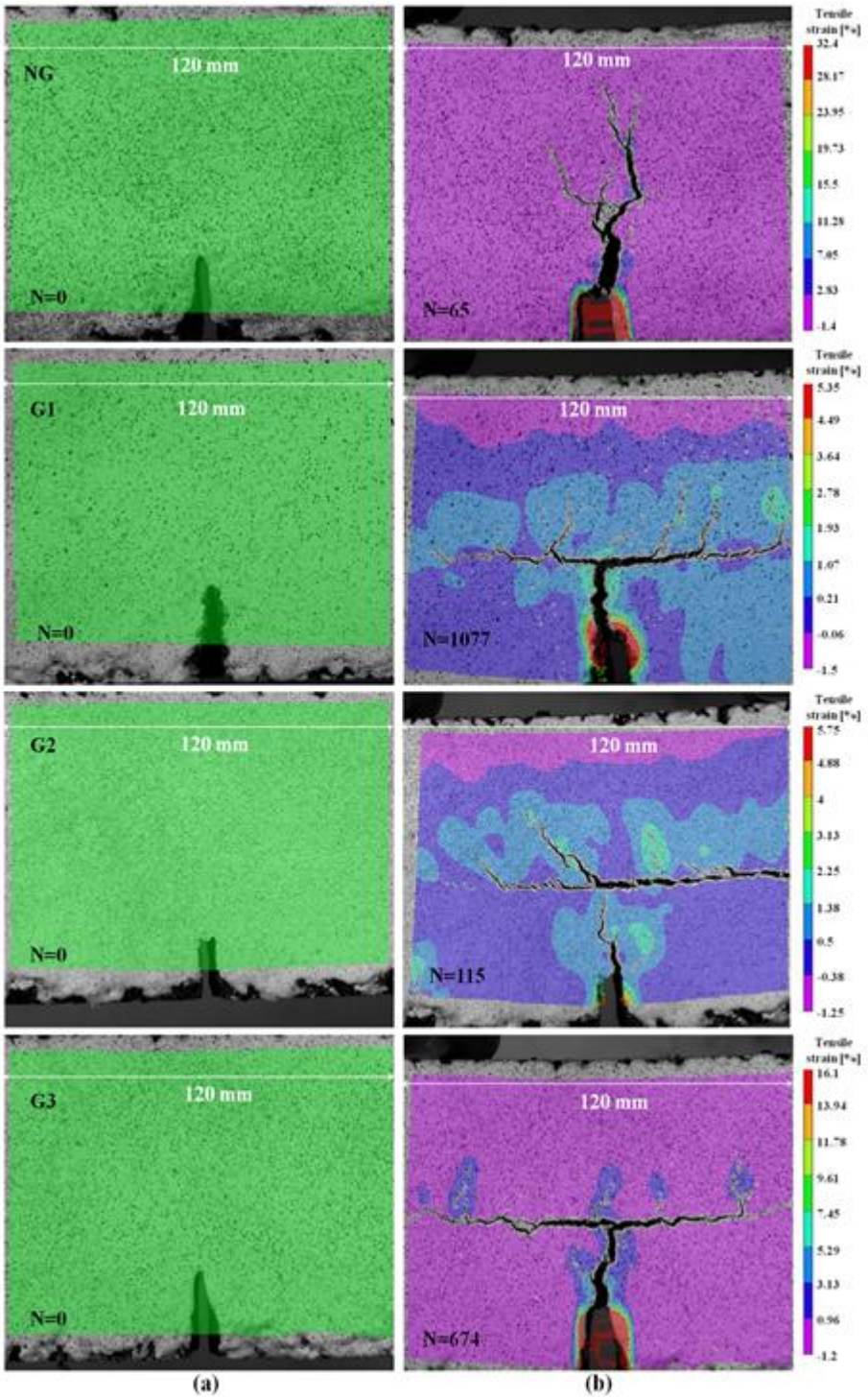

Fig. 11: Typical DIC results for samples with 25 mm crack depth (a) Before testing, (b) Tensile strain contours at failure

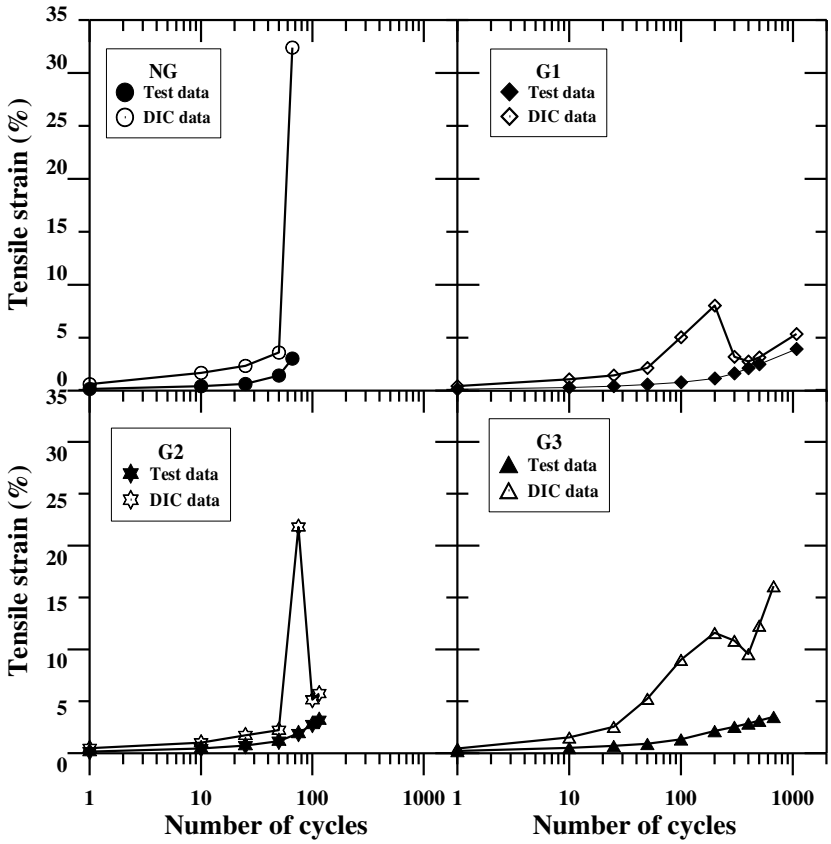

Fig. 12: Tensile strains measured from DIC analysis and test data for sample with 25 mm crack depth (a) NG; (b) G1; (c) G2; and (d) G3

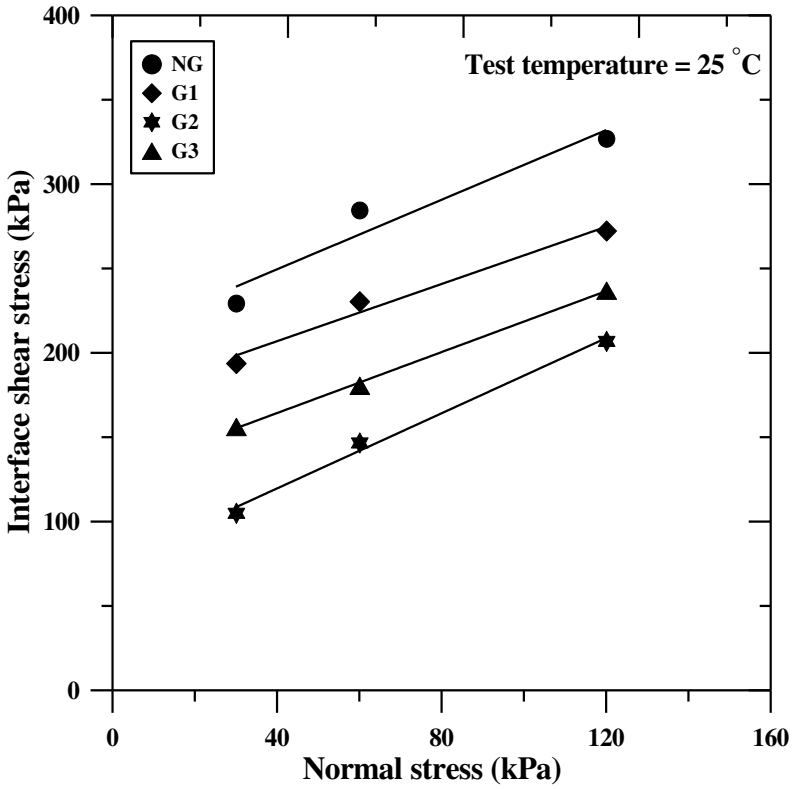

Fig. 13: Variation of interface shear stress with normal stress at a temperature of 25 °C

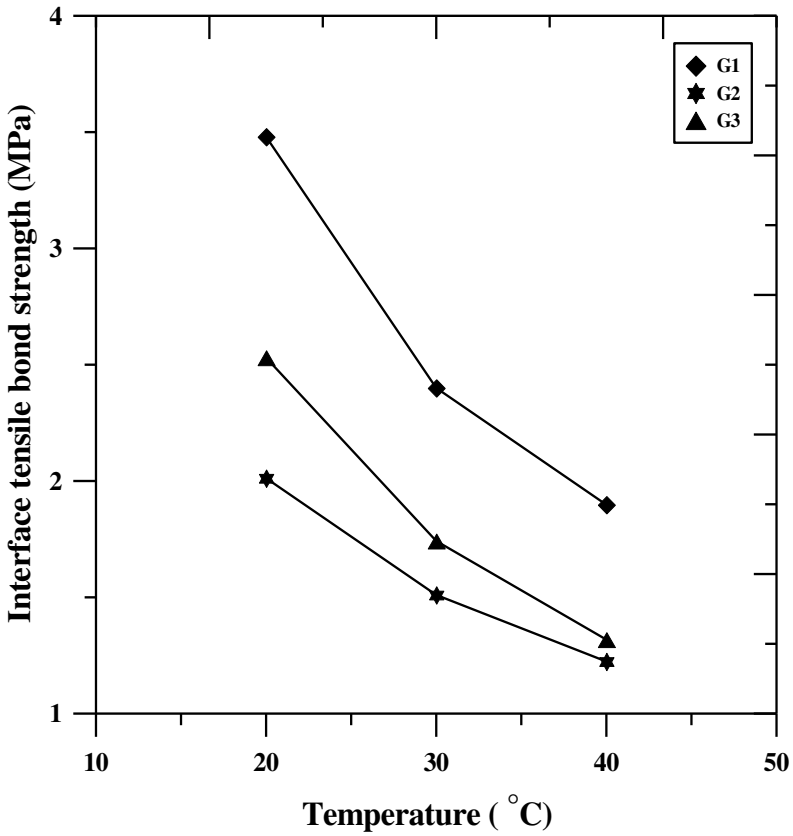

Fig. 14: Variation of interface tensile bond strength with temperature